Proceedings of the 26th International Conference on Offshore Mechanics and Arctic Engineering
OMAE2007
June 10-15, 2007, San Diego, California, USA

OMAE2007-29100

REELING OF TIGHT FIT PIPE (TFP)

E. S. Focke
Heerema Marine Contractors
Vondellaan 55, 2332 AA, Leiden, The Netherlands,
Tel: +31 (0)71 5799161,
efocke@hmc-heerema.com

E. Karjadi
Heerema Marine Contractors
Vondellaan 55, 2332 AA, Leiden, The Netherlands,
Tel: +31 (0)71 5799637
ekarjadi@hmc-heerema.com

A. M. Gresnigt
Delft University of Technology
P.O.Box 25,
Delft,
The Netherlands,
Tel: +31 (0)15 2788833,
a.m.gresnigt@tudelft.nl

J. Meek
Delft University of Technology
P.O.Box 25,
Delft,
The Netherlands,
Tel: +31 (0)15 2784777,
j.meek@offshore.tudelft.nl

H. Nakasugi
Kuroki Tube & Pipe Co. Ltd.
Sanyu Bldg 9F
2-30-17, Higashi-Kamata,
Ohta-Ku, Tokyo 144 - 0031, Japan
Tel: +81 (0)3 57101310
hajime.nakasugi@kuroki-tokyo.co.jp

ABSTRACT

A 12.75 inch outer diameter single walled pipe bending test was executed and theoretical and FE analysis of this test was performed as preparation for 12.75 inch outer diameter TFP bending tests. The main objective of the TFP bending tests was to determine the initiation and degree of liner wrinkling occurring during the TFP spooling-on phase when simulating the reeling pipelay installation method. Due to lack of a definition of liner wrinkling initiation, the crossing of a certain threshold of the liner wrinkle height was defined as liner wrinkling initiation. The bending tests results indicated that (1) the extent of liner wrinkling decreased if TFP with a high mechanical bonding strength was used. (2) The presence of a circumferential weld in the highly bonded TFPs initiated higher liner wrinkles at lower curvatures than in case no circumferential weld was present. (3) The ERW outer pipe longitudinal weld did not result in higher liner wrinkles. API residual compressive stress tests showed that the initial mechanical bonding strength in the 12.75 inch TFP used in this research was significantly reduced, irrespective of whether a high or a low initial mechanical bonding strength had been used prior to spooling-on. These findings justify further research into this phenomenon as the eventual mechanical bonding strength after reeling installation may be vital for its anticipated application during operation.

INTRODUCTION

Hydrocarbons can contain H_2S, CO_2 and other corrosive products that require corrosion resistant alloys (CRA) for tubing in the wells and for the pipelines (flowlines) to the treating stations. A promising possibility to reduce costs is the concept of Tight Fit Pipe (TFP), which is a double wall pipe where a CRA liner is mechanically fitted inside a carbon steel outer pipe through a thermo-hydraulic manufacturing process [1] (Fig. 1).

If it were possible to install TFP by reeling, it will be an attractive new option for corrosive fields. Reeling of TFP is however not yet proven technology. An important subject is the risk of liner wrinkling [2], which is most likely to occur during the spooling-on phase of the reeling process because maximum bending occurs in this phase.

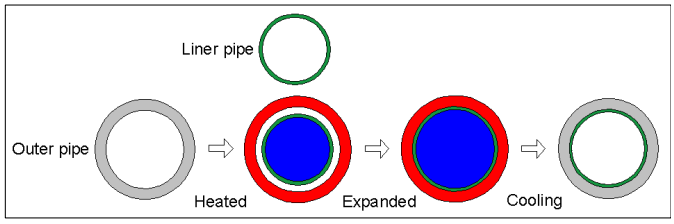

Figure 1 TFP manufacturing process

This paper describes the research performed in order to investigate the initiation and degree of liner wrinkling as well as the ovalisation of the TFP during spooling-on in the reeling process, both theoretically and experimentally; the latter by performing full scale bending tests.

In order to prepare for the full scale bending testing of TFP, a bending rig had to be built. Axial compression tests on TFP [3] and small scale reeling tests on 22 mm outer diameter single walled pipe [4] have been executed prior to building the full scale bending rig because the experimental and theoretical results from these tests aided in the design of the full scale bending rig. By identical bend testing a 12.75 inch single walled pipe prior to bend testing the 12.75 inch TFPs, the fit for purpose of the full scale bending rig was assessed. The bending test on the single walled pipe and the bending tests on TFPs are reported in this paper.

NOMENCLATURE

a:	liner wrinkle height [mm]
d, $d_{L;o}$; $d_{O;o}$:	single walled pipe, liner pipe and outer pipe outer diameter [mm]
f_0:	initial pipe ovalisation [%]
f_{MBS}:	pipe ovalisation when bent on reel [%]
F_{HC}:	hydraulic cylinder force [kN]
$F_{HC;A}$, $F_{HC;P}$:	axial and transverse components of the hydraulic cylinder force [kN]
$F_{HC;x}$, $F_{HC;y}$:	x and y components of the hydraulic cylinder force [kN]
L/m:	half wave length of the local buckle [mm]
M:	moment [kNm]
$M_{P;TEST-1}$:	plastic bending moment capacity of pipe TEST-1 [kNm]
$M_{P;TEST-2}$:	plastic bending moment capacity of pipe TEST-2 [kNm]
t, t_L, t_O:	single walled pipe, liner pipe and outer pipe wall thickness [mm]
U_1, U_2, U_3:	pipe movements in x, y, z direction [mm]
β:	angle identifying the length of pipe in contact with the reel [rad]
γ:	angle between the pipe and the hydraulic cylinder [rad]
$\Delta d_{L;a;TFP}$:	change in the average diameter of the liner due to the radial contact pressure [mm]
ε_b:	bending strain [%]
κ:	curvature [1/m]
σ_C:	radial contact pressure between the liner and the outer pipe (mechanical bonding) [MPa]
$\sigma_{L;res}$:	residual liner hoop stress [MPa]
ζ:	change in the hydraulic cylinder orientation during the bending test [rad]
CRA:	Corrosion Resistant Alloy
ERW:	Electric Resistance Welded
FE:	Finite Element
ICP:	Initial Contact Point
TFP:	Tight Fit Pipe

FULL SCALE BENDING TEST ON 12.75 INCH SINGLE WALLED PIPE

Experimental Test Set-up

Although the manufacturing process aims to fabricate pipes with identical material and geometric properties, there will always be some variation per pipe element [5]. This results in difference in bending strength properties of the pipes. If by chance a pipe with a high bending moment capacity (strong pipe) is spooled on the reel prior to a pipe with less bending moment capacity (weak pipe), buckling may occur in the weaker pipe close to the weld due to strain concentration at that location (Fig. 2).

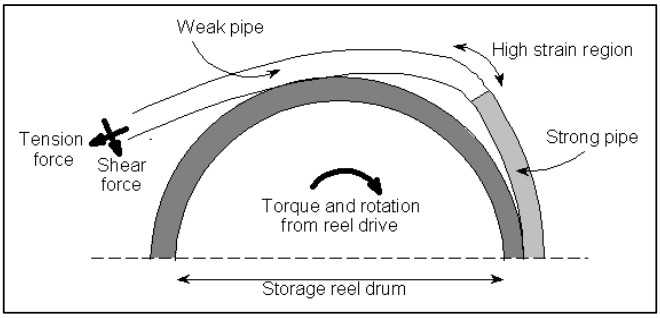

Figure 2 Effect of variation in material and geometrical properties of reeled pipes

In order to simulate reality as much as possible, the test piece that was bent in the test rig consisted of a 21.77 mm thick, 12.75 inch outer diameter pipe (TEST-1) connected by an overmatching weld to an 18.65 mm thick, 12.75 inch outer diameter pipe (TEST-2). Pipes TEST-1 and TEST-2 were connected to each other in such way that TEST-1 was bent prior to TEST-2. The pipe wall of pipe TEST-1 was machined next to the weld in order to reduce the risk of early buckling in pipe TEST-2. The test pipe (TEST-1 connected to TEST-2) was attached by flanges to a re-usable pipe in order to fit in the bending rig (Fig. 3).

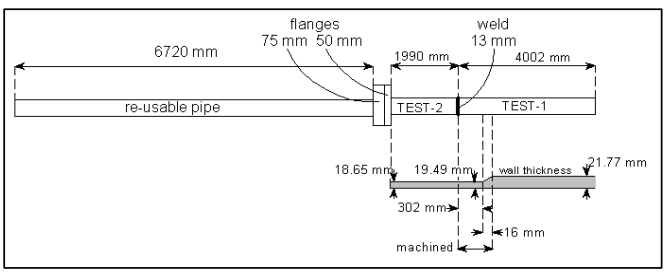

Figure 3 Test piece bent in the full scale bending rig

In the full scale bending rig the test pipe was bent stepwise to smaller bending radii (Fig. 4 and Fig. 5). Reel radii available were 9 m, 8 m, 7.5 m, 7 m, 6.5 m, 6 m, 5.5 m and 5 m.

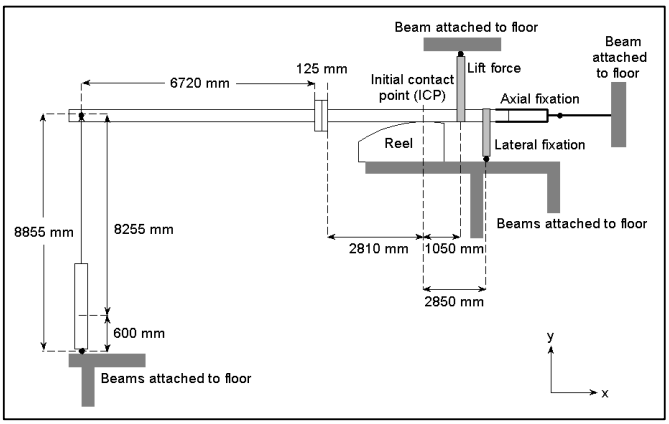

Figure 4 Schematic overview of the full scale bending rig

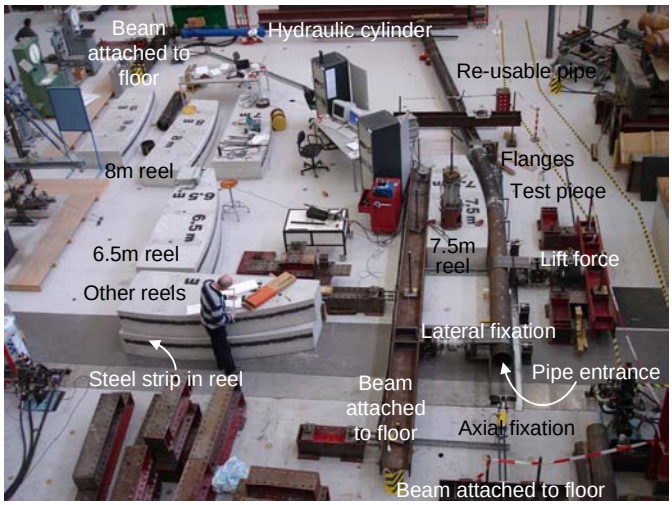

Figure 5 Full scale bending rig in the laboratory

A "lift" force was applied in the full scale bending rig. This "lift" force on the pipe reduced the initial reaction force of the reel on the pipe in the beginning of the test at the initial contact point (ICP). The initial reaction force of the reel on the pipe in the beginning of the test, acting as a transverse force on the pipe, was expected to enhance ovalisation and could cause unintended local buckling in the beginning of the test [6], [7].

Finite Element Analysis Model in ABAQUS

The full scale bending rig has been modelled in ABAQUS FE analysis software [8] and simulated the stepwise bending and elastic unloading process of the test pipe against successively decreasing radii sizes (Fig. 6).

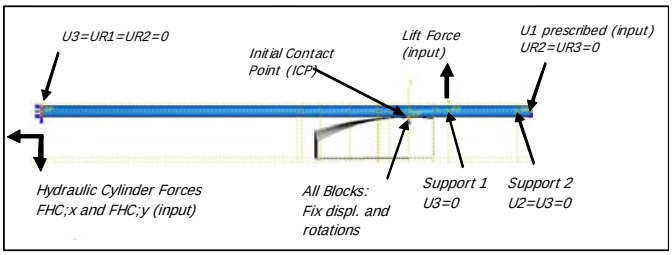

Figure 6 FE Model of the full scale bending rig in ABAQUS

The test pipe was modelled using 4-node shell elements (ABAQUS S4R elements). The horizontal and vertical components of the hydraulic cylinder force ($F_{HC;x}$, $F_{HC;y}$), the lift force at support 1 and the axial displacement U_1 of the test pipe at the axial fixation point, were obtained from the test measurements and were used as input (Fig. 6). Unless rotation was allowed, the reels were restrained at the ICP in all three translational and rotational degrees of freedom. Further details of the FE modelling and analysis can be found in Ref. [9].

Comparison between Test Results, FE Calculations and Analytical Predictions

During the test three main areas of interest were monitored.

1. Forces in the bending rig
2. Ovalisation of the pipe
3. Local buckling of the pipe

1. Forces in the bending rig

In the bending rig, the hydraulic cylinder force, the forces in the axial and the lateral fixation points (i.e. the axial and the lateral fixation point forces) and the lift force were measured using load cells (Fig. 4 and Fig. 5).

Two situations were distinguished in the bending test [4]. In Situation I, the hydraulic cylinder force increases until the plastic bending moment has been reached in the ICP. In Situation II (Fig. 7) more pipe comes in contact with the reel reducing the distance between the reel and the hydraulic cylinder thereby increasing the hydraulic cylinder force. In Situation II the orientation of the hydraulic cylinder changes (angle ζ). Because the orientation of the hydraulic cylinder (angle ζ) changes and more pipe length comes in contact with the reel (angle β), the x and y components ($F_{HC;x}$, $F_{HC;y}$) as well as the axial and perpendicular components ($F_{HC;A}$, $F_{HC;P}$) change during the test (Fig. 7).

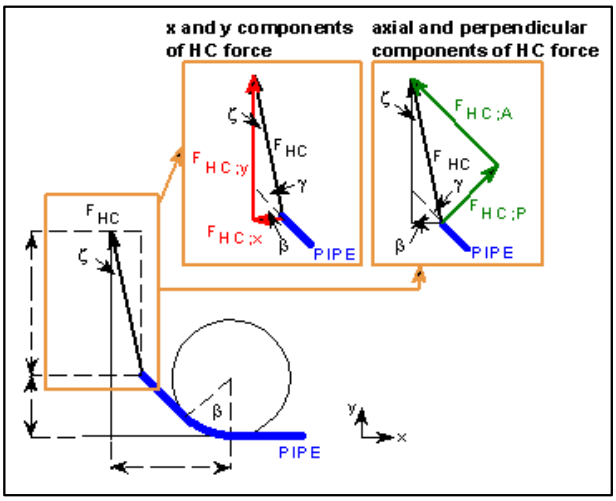

Figure 7 Force components of the hydraulic cylinder

The lateral fixation point force increases in Situation I but remains constant in Situation II because the distance between the ICP and the fixation point is constant (Fig. 4).

Equations used to predict the hydraulic cylinder force and its components as well as the lateral fixation point force in Situations I and II can be found in Ref. [4]. In Fig. 8 a comparison is shown between the predicted and the measured hydraulic cylinder force and lateral fixation point force at the end of Situations I and II (for the 9 m radius reel).

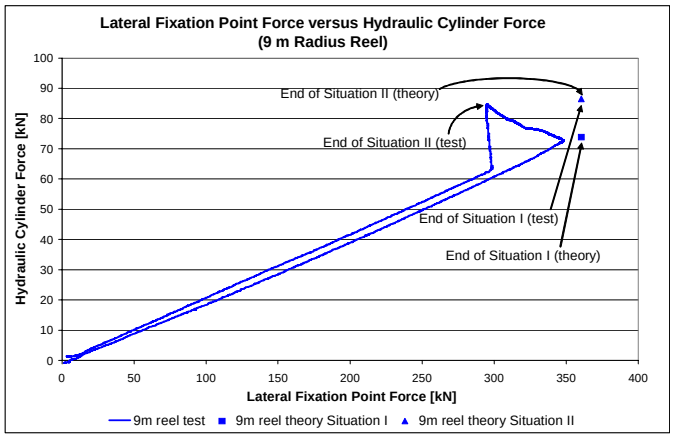

Figure 8 Hydraulic cylinder force versus lateral fixation point force

The theoretical values of the hydraulic cylinder force at the end of Situations I and II as well as the lateral fixation point force at the end of Situation I correlate well with the experimental values (Fig. 8). It has been theoretically predicted and experimentally proven in the small scale reeling tests (with and without a lift force) that the lateral fixation point force remains constant, once the plastic bending moment has been reached at the ICP at the end of Situation I [4]. However, Fig. 8 shows that the lateral fixation point force starts decreasing at the end of Situation I, resulting at the end of Situation II in the experimental fixation point force to be overestimated by the theoretical prediction. The decrease of the lateral fixation point force at the end of Situation I can be explained by the presence of the difference in bending moment capacity of the pipes at both sides of the weld, $M_{P;TEST-1}$ and $M_{P;TEST-2}$ (Fig. 9). Pipe TEST-2, in contact with the reel in Situation II can not have a bending moment larger than its plastic bending moment capacity $M_{P;TEST-2}$. The bending moment in pipe TEST-1 at the end of Situation I ($M_{P;TEST-1}$) had thus to be reduced in Situation II from $M_{P;TEST-1}$ to $M_{P;TEST-2}$ in order to accommodate $M_{P;TEST-2}$ in pipe TEST-2. The fixation point force thus also reduced in value in the bending test after Situation I.

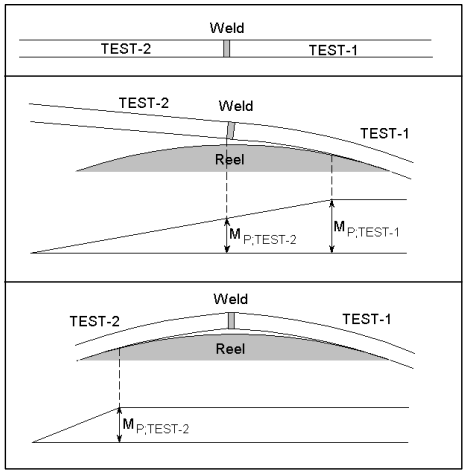

Figure 9 Bending of the single walled pipe

The lift force was removed from the test set-up prior to performing TFP bending tests. It appeared not needed to avoid excessive ovalisation and local buckling in the beginning of the test, while it does complicate the FE analysis.

2. Ovalisation of the pipe

Ovalisation of the test pipe was measured by hand prior to bending and stepwise after bending both by hand and by the ovalisation meters OM1 to OM4 (Fig. 10).

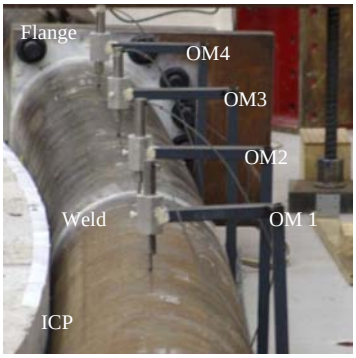

Figure 10 Ovalisation Meters

The stiffening effect of the flanges reduces ovalisation in the adjacent cross sections. This effect and effects of load introduction at the ends of the reel and the lift force had an influence on the ovalisation at OM1 and OM4. The ovalisations at OM2 and OM3 in the central part (measuring length) were not influenced by these end effects. In this paper only the results from OM2 and OM3 are discussed (Table 1). Ovalisation in the TFP tests was measured by a larger amount of ovalisation meters and hand measurements located in the test region.

The ovalisation meter consisted of a steel U frame attached to the bottom of the pipe. A displacement meter in the top of the frame measured the vertical increase of the outer diameter of the pipe. Only the increase in the outer diameter in the vertical plane could be measured due to the presence of the reel. During ovalisation, the decrease in diameter in the horizontal plane is not identical to the (measured) increase in diameter in the vertical plane. A ratio was defined between the horizontal and the vertical change in the diameter measured by hand after each bending stage. The horizontal change in diameter at maximum bending was determined by multiplying the vertical change in diameter measured by the ovalisation meter by this ratio. Ovalisation at maximum bending was thus determined by the ovalisation meters. This value of ovalisation at maximum bending was compared to a prediction for ovalisation (Table 1) stated in the DNV OS F101 code [10].

$$f_{MBS} = f_0 + \left(0.030 \cdot \left(1 + \left(\frac{d}{120 \cdot t} \right) \right) \cdot \left(2 \cdot \varepsilon_b \cdot \frac{t}{d} \right)^2 \right) \quad (1)$$

Eq. (1) underestimates values for ovalisation measured in the bending test (Table 1). This can be explained by the fact that Eq. (1) is based on test results from four point bending tests in which the reaction force of the reel on the pipe, enhancing ovalisation, was not taken into account [11], [12]. Note that the pipe was bent on the 9 m reel in three steps due to fact that the length of the hydraulic cylinder stroke was not long enough to pull the TFP completely on the reel in one go.

Table 1 Measured and predicted ovalisation

	TEST-1 (OM2) f_{MBS} [%]	TEST-2 (OM3) f_{MBS} [%]	Eq. (1) OM2 f_{MBS} [%]	Eq. (1) OM3 f_{MBS} [%]
9m (1)	0.19	0.09	1.16	1.29
9 m (2)	1.57	2.50	1.16	1.29
9 m (3)	1.54	2.55	1.16	1.29
8 m	1.40	3.47	1.47	1.63
7.5 m	2.04	3.83	1.67	1.85
7 m	2.39	4.64	1.91	2.11
6.5 m	2.56	4.99	2.20	2.44
6 m	2.41	5.29	2.57	2.86
5.5 m	2.91	5.71	3.05	3.38
5 m	3.41	6.72	3.67	4.07

Results of a comparison of ovalisation measured by ovalisation meters OM2 and OM3 with the ovalisation from the FE analysis is shown in Fig. 11 and Fig. 12. The ovalisation has been plotted as a function of the loading and unloading sequence steps (1 to 20). An uneven step number indicates a step of bending loading the pipe on the reel while an even step number indicates the step of elastic unloading. Note that the pipe was bent on 9 m reel three steps (step 1 to 6). Step 7 to 20 indicated bending and elastic unloading steps of the pipe against 8 m to 5 m radius reels. Prediction of ovalisation using Eq. (1) is also shown in Fig. 11 and Fig. 12.

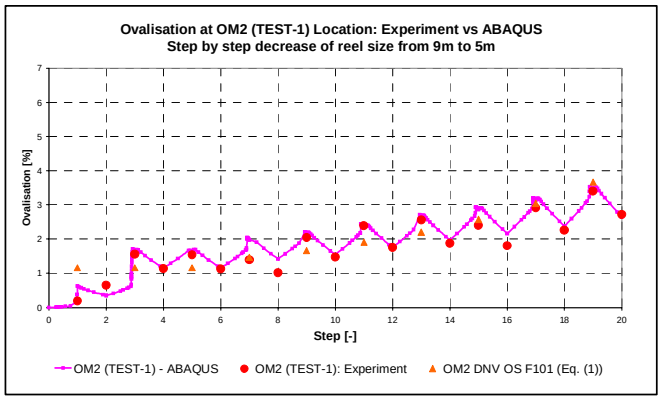

Figure 11 Comparison of ovalisation OM2 (machined TEST-1); experiment and FE analysis

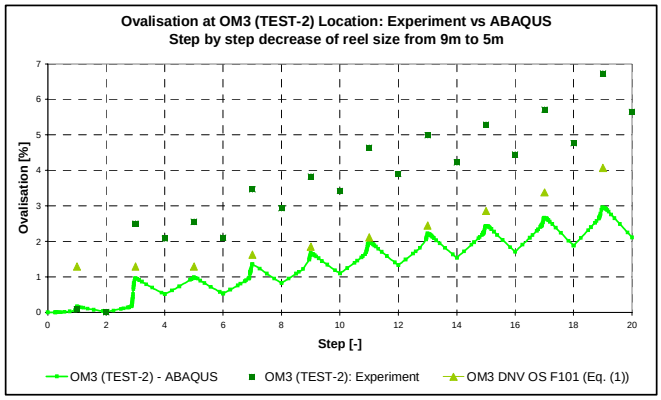

Figure 12 Comparison of ovalisation OM3 (TEST-2); experiment and FE analysis

Values for pipe ovalisation in the experiment and from the FE calculations are in good agreement at the OM2 location (Fig. 11). Fig. 12 shows the pipe ovalisation from the experiment and from the FE analysis at the OM3 location. The final pipe ovalisation at the elastic unloading step after bending the pipe on the 5 m radius reel shows a rather big difference between the experiment and the FE calculations. The difference was initiated at step 3 of the simulation when bending the pipe on the 9 m radius reel for the second time. At this step, the ovalisation of the pipe at the OM3 location was 1.5 % in value underestimated by the FE analysis. The reason of the

underestimation of the pipe ovalisation in the FE analysis is due to an idealization of the fixation of reels (no translational and rotational movements) in the model. During the experiments it was found that the reel rotated first clockwise when the pipe was only in contact with the reel at the ICP (Fig. 4 and Fig. 5). This rotation was mainly due to the reel rotating slightly around its rotation point towards the beam, located behind the reel in order to fill the small gap between the reel and the beam. This gap was the result of the fact that it was impossible in practice to align the reel completely with the beam located behind it. The rotation of the reel was possible due to the fact that the rods, connecting the reel to the floor under pretension, were able to move slightly within the holes, through which the rods connected the reel to the floor. By increasing the hydraulic cylinder force more pipe came in contact with the reel and the reel was rotated back (counter clockwise) past its original position and bent the supporting beam (Fig. 13).

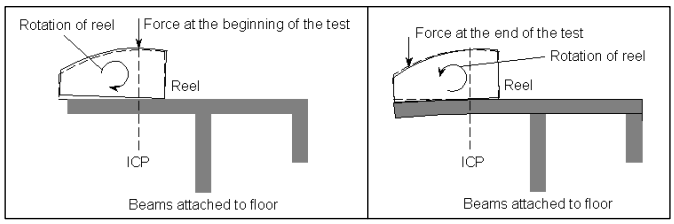

Figure 13 Rotation of the reel during the bending test

The rotation of the reel influenced which part of the pipe length was in contact with the reel and would thus be submitted to the reaction force of the reel. Ovalisation in OM3 increased from 0.96 % (Fig. 14) to 2.34 % (Fig. 12 and Fig. 13) due to the fact that the reel rotation caused the OM3 location to come in contact in with the reel while this location would not be in contact with the reel if no reel rotation occurred.

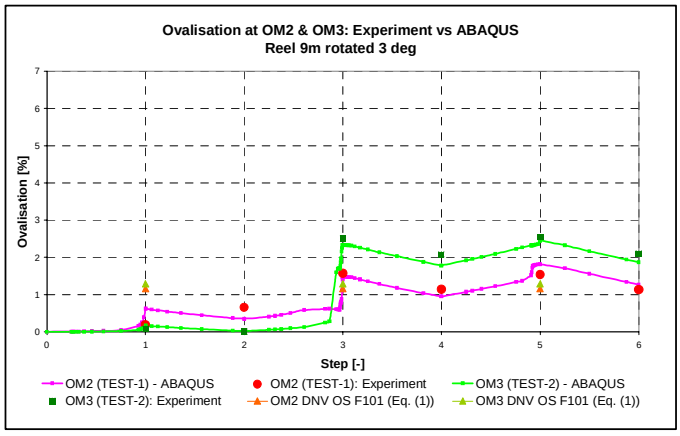

Figure 14 Comparison of ovalisation OM2 and OM3 for 9 m radius reel with 3° clockwise rotation; experiment and FE analysis

In this simulation (Fig. 14) the 3 degrees clockwise rotation of the reel was assumed to take place at step 3 when bending the pipe on 9 m radius reel. It can be seen that the results between pipe ovalisation from the experiment and the FE calculation compare well when a rotation of the reel is allowed during the FE analysis.

In subsequent TFP bending tests, the reel rotation was minimised by locating two extra beams behind the concrete block.

3. Local buckling of the pipe

A local buckle was first noticed in the weaker pipe (TEST-2) after bending the pipe on the 6 m radius reel (Fig. 15).

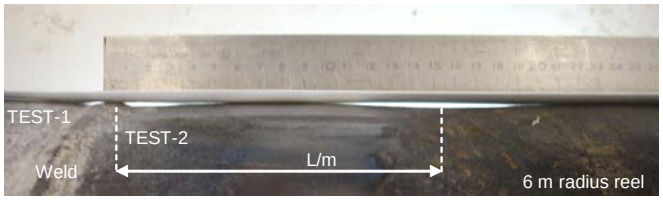

Figure 15 Local buckling of the single walled pipe

The prediction of the critical buckling strain by Murphy and Langner [11], by Gresnigt [7] and by DNV Offshore Standard OS-F101 [10] exceeded the experimental buckling strain (Table 2).

Table 2 Comparison of predicted and experimentally determined critical buckling strain

ε_b [%]	ε_{cr} Murphy & Langer [%]	ε_{cr} Gresnigt [%]	ε_{cr} DNV [%]
2.63	2.88	2.81	3.89

It should be noted that in reality the local curvature and the bending strain were larger because of the extra bending in the weaker pipe TEST-2 (Fig. 9). Furthermore, the depth of the local deformation was still rather small and it is not clear whether this should be defined as local buckling (Fig. 15). Usually, local buckling is defined as the point in the moment curvature diagram where due to the local deformations in the wall, the bending moment starts decreasing. Especially in thick walled pipes the bending moment still increases after initiation of local buckles.

The half wave length (L/m) and the height (a) of the buckle were approximately 150 mm and 1.1 mm, respectively, both measured after bending the pipe on the 5 m reel. The FE calculation predicted a length of approximately 140 mm.

FULL SCALE BENDING TESTS ON 12.75 INCH TFP

The experience with the full scale bending test on the 12.75 inch single walled pipe has contributed to the preparation of the full scale bending tests on 12.75 inch TFPs.

TFP Test Pipes in Bending Rig

The way of testing the 12.75 inch outer diameter TFP test pipes (with a 3 mm, 316 L liner and a 14.3 mm, X65 outer pipe) was identical to the single walled pipe bending test.

Five TFP specimen (identified as TFP-1, TFP-2, TFP-3, TFP-4 and TFP-5) consisted of a 3.44 m, 12.75 inch TFP connected by a weld on one side to a 2.5 m, 12.75 inch single walled pipe and on the other side to the flange. Two TFP test pieces (identified as TFP-6 and TFP-7) with a TFP circumferential weld (Fig. 16) consisted of two pieces of 12.75 inch TFP, each 1.72 m in length (making up 3.44 m TFP) connected to a 2.5 m, 12.75 inch single walled pipe on one side and a flange on the other side (Fig. 17 and Table 3).

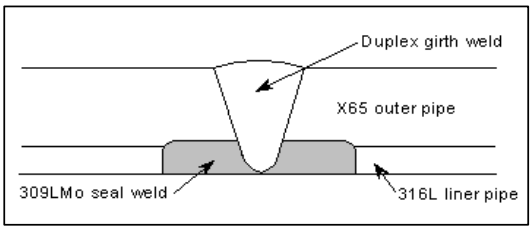

Figure 16 TFP weld

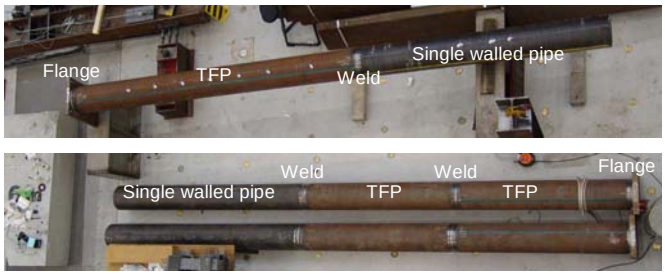

Figure 17 TFP test pipes without (top) and with (bottom) a TFP circumferential weld

Table 3 Overview of TFP test pipes

	$\sigma_{L;res}$ [MPa]	ERW Outer Pipe Weld	TFP Circumferential Weld	Bending to Reels
TFP-1	189	CZ	no	stepwise
TFP-2	189	CZ	no	once
TFP-3	189	CZ	no	stepwise
TFP-4	53	NL	no	stepwise
TFP-5	53	CZ	no	stepwise
TFP-6	189	CZ & TZ	yes	stepwise
TFP-7	189	CZ & TZ	yes	stepwise

Note:
CZ = Compression zone; NL = Neutral line; TZ = Tension zone

The objective of bending the TFP tests pipes was to investigate the initiation and the degree of liner wrinkling as well as the ovalisation of the TFP during spooling-on in the reeling process. By comparing liner wrinkling of TFP-1, TFP-2 and TFP-3 with the liner wrinkling of TFP-4 and TFP-5, the influence of (1) the mechanical bonding strength between the TFP liner and outer pipe on liner wrinkling could be investigated (Table 3). By comparing liner winkling in TFP-4 and TFP-5, (2) the influence of the ERW longitudinal outer pipe weld on liner wrinkling could be investigated. By comparing TFP-1, TFP-2 and TFP-3 with TFP-6 and TFP-7, (3) the influence of the TFP circumferential weld on liner wrinkling could be found. By comparing liner wrinkling of TFPs TFP-2 and TFP-3, the difference in bending in “one go” to a reel radius (5.5 m) versus stepwise bending on this reel radius can be determined (4).

Comparison between Experiment and Theory

During the test four main areas of interest were monitored.

1. Forces in the bending rig
2. Strain and curvature of the TFP
3. Ovalisation of the TFP
4. Local buckling of the TFP

1. Forces in the bending rig

The hydraulic cylinder force and the lateral fixation point force, predicted using equations from Ref. [4], correlated well with experimental results.

2. Strain and curvature of the TFP

A large number of strain gauges were applied to the tension and compression zone of the TFP. In the compression zone they were located just under the contact line with the reel to avoid squeezing. Also two curvature meters were attached to the pipe (Fig. 18). The theoretically predicted global bending strain and the measured strain data obtained from the curvature meters and the strain gauges, correlated well.

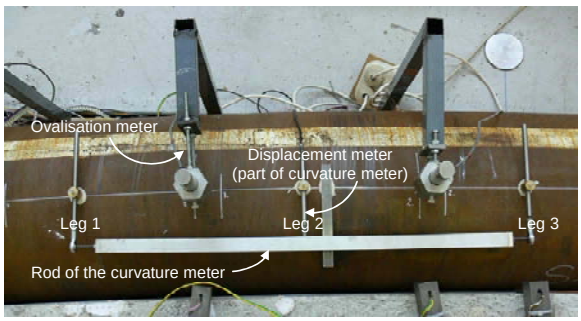

Figure 18 Curvature meter

Strain concentrations in TFPs TFP-6 and TFP-7 in the compression zone were measured by strain gauges surrounding the weld. The measured bending strains in the strain gauges varied around the weld (Table 4). This could be the result of differences in geometry (weld and pipe) and in material (X65 parent material and duplex weld consumable). Also the welding

heat input, the residual stresses due to the welding heat input and the Bauschinger effect could have contributed to the variation of the measured strains around the weld.

Table 4 Strains around the TFP circumferential weld (TFP-7) when pipe is bent to the 5.5 m radius reel

Distance from weld [mm]	80	30	15	Weld	15	30	80
5.5 m reel	-2.18	-1.97	-5.48	-3.71	-3.84	-2.53	-2.67

3. Ovalisation of the TFP

As in the 12.75 inch single walled pipe bending test, the experimental TFP ovalisation was underestimated by Eq. (1) using only the outer pipe wall thickness as well as assuming the liner and the outer pipe wall thicknesses "added", representing one single wall thickness (Fig. 19). This underestimation is also explained by the DNV Offshore Standard OS-F101 code disregarding the reaction force of the reel on the pipe.

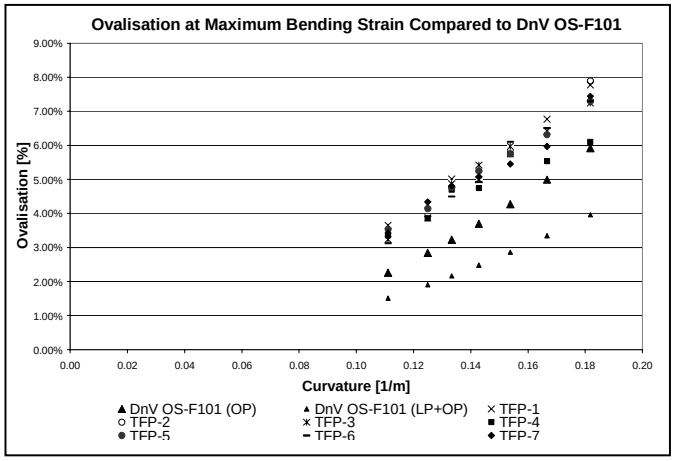

Figure 19 Comparison of experimental and theoretical ovalisation

The maximum ovalisation measured after spooling-on in the full scale bending test of 12.75 inch TFP exceeded the 3.0 % allowable threshold for ovalisation (after installation) as stated in DNV OS F101 code [10], after bending it on the 7 m radius reel [13]. What ovalisation should be allowed after unreeling and straightening depends on the loads (e.g. water depth) and the required safety margin. Reduction of ovalisation can be obtained by increasing the reel radius and / or the diameter to wall thickness ratio.

3. Local buckling of the TFP

In the bending tests liner wrinkling was clearly present while local buckling of the outer pipe was not. Changes of the operational pressure may increase and decrease the sizes of liner wrinkles. This may affect the fatigue life and can possibly cause fractures to develop. Apart from affecting the fatigue behaviour, another incentive to minimise liner wrinkling is that they could obstruct a pig from passing through the pipe.

A special laser wagon has been developed to scan the inside of the TFP and measure liner wrinkles (Fig. 20) prior, during and after bending the TFP on the reel.

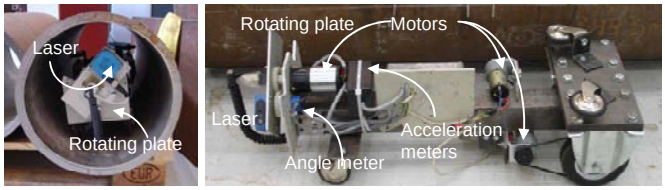

Figure 20 Laser wagon

Scans, made by the laser wagon, represent the radial displacements of the liner wall. The locations of the liner wrinkles were determined from this laser scan (Fig. 21). The blue regions in the compression zone indicate liner wrinkles.

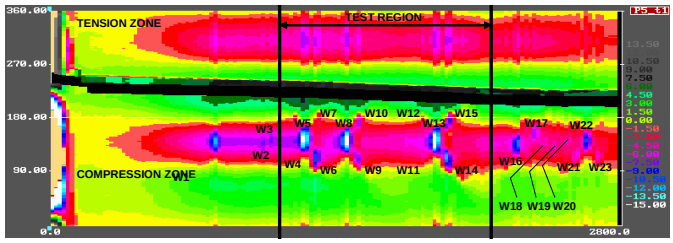

Figure 21 Laser radial displacements scan of TFP-4

As mentioned earlier, one of the objectives of the testing was to determine liner wrinkling initiation of which there is currently no clear definition. A suggestion is to define initiation of liner winkling as crossing a certain threshold of the liner wrinkle height. This threshold for the liner wrinkle height could be based on its influence on fatigue life reduction or the size of a pig and its ability to pass liner wrinkles of a certain height. Research into this subject still has to be performed.

Since the liner wrinkle height was used as a measure for the liner wrinkle initiation in this research, the liner wrinkle height had to be obtained from the data provided by the laser wagon. A consistent method of determining the liner wrinkle height needed to be established: the bottom of the liner wrinkle was defined as the intersection of two lines (Fig. 22): (1) the line connecting the valley in front of the top of liner wrinkle (prebottom) with the valley behind the top of liner wrinkle (postbottom) and (2) the line dropped perpendicularly down from the top on the pipe axis. The difference in height between this intersection point and the top of the liner wrinkle was defined as the liner wrinkle height.

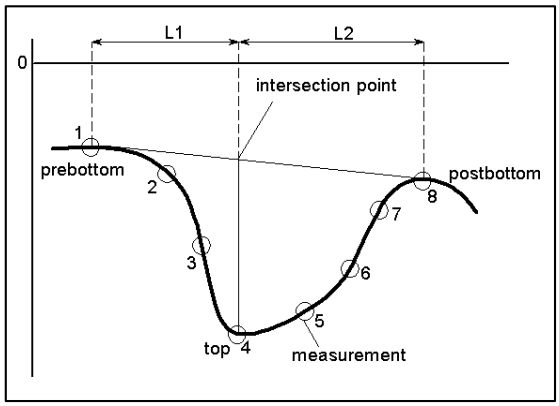

Figure 22 Definition of the liner wrinkle height

From the test results, several observations can be made in regard to liner wrinkling:

(1) Mechanical bonding strength

For TFPs without a TFP circumferential weld, Fig. 23 shows that an increase in the mechanical bonding strength indicates a decrease in the liner wrinkle height of the largest residual liner wrinkle. The height of the residual liner wrinkles in a TFP with a high residual liner hoop strength are more or less exponentially dependent on the curvature while the residual liner wrinkles in a TFP with a low residual liner hoop strength are more linearly dependant on the curvature.

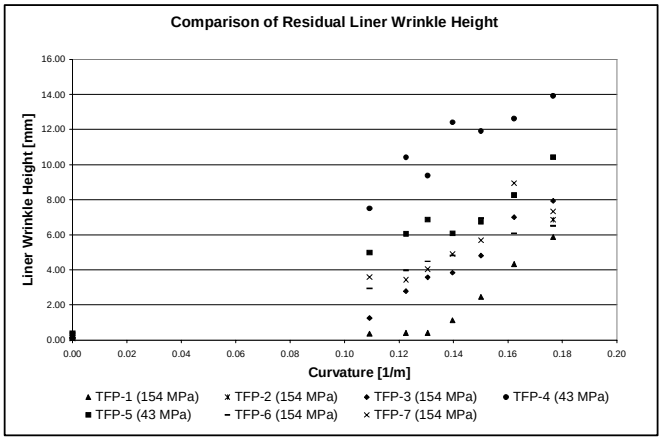

Figure 23 Comparison of residual liner wrinkle height for different curvature

A higher mechanical bonding strength also results in less liner wrinkles with a different distribution over the TFP inner surface (TFPs without a TFP circumferential weld; Fig. 24).

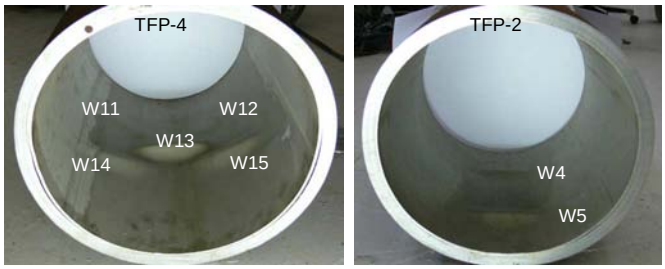

Figure 24 Liner wrinkles in TFPs with a low (left) and high (right) mechanical bonding strength

This decrease in liner wrinkling at higher mechanical bonding strength can be explained by the fact the higher radial contact stress between the TFP liner and outer pipe (σ_C) results in a higher friction between the TFP liner and outer pipe. This higher friction avoids liner material to "feed in" the liner wrinkle. At a certain curvature, this results in less liner wrinkling for TFPs with a high mechanical bonding strength than for TFPs with a lower mechanical bonding strength.

(2) ERW outer pipe longitudinal weld

It can be seen in Fig. 23 that the ERW longitudinal outer pipe weld did not cause higher liner wrinkles at lower curvatures. This may be explained by the fact that this weld is continuous along the length of the TFP and did not function as a local imperfection, triggering liner wrinkling.

(3) TFP circumferential weld

The presence of a TFP circumferential weld in highly bonded TFPs resulted in higher liner wrinkles for lower curvatures than when no TFP circumferential weld was present (Fig. 23). The liner wrinkling behaviour of the highly bonded TFPs with a TFP circumferential weld depended more or less linearly on the increasing curvature. Highly bonded TFPs with no TFP circumferential weld were more exponentially dependent on the increasing curvature. The distribution of the liner wrinkles of the highly bonded TFPs with a TFP circumferential weld showed a distribution of the liner wrinkles similar to the lower bonded TFPs without a TFP circumferential weld (Fig. 22). In other words, the behaviour of the highly bonded TFPs with a TFP circumferential weld resembled the behaviour of the less bonded TFPs without a TFP circumferential weld at the same curvatures.

The occurrence of higher liner wrinkles at lower curvature for highly bonded TFPs with a TFP circumferential weld may be explained by the fact that the presence of the weld resulted in a less even distribution of the contact stress between the reel and the TFP during bending. This was the result of the fact that the TFP was in contact with the reel at the location of weld cap and some distance further along the reel. The locally higher contact forces there where the TFP came in contact with the reel again further along the reel from the weld cap resulted in small

indentations in the pipe wall that triggered the initiation of the wrinkles (tests TFP-6 and TFP-7).

(4) Stepwise bending versus bending in "one go"

Comparing wrinkle height of the largest liner wrinkle for TFP-2, bending in one go, and TFP-3, stepwise bending, indicates that step by step bending does not result in significantly higher liner wrinkles (Fig. 23). Since there was also no significant difference in ovalisation between TFP-2 and TFP-3, the test method of step by step bending to find the initiation of liner wrinkling can be concluded to be an adequate and acceptable testing procedure.

LINER WRINKLING PREDICTION

The residual liner wrinkle height (a) as a result of spooling-on depends on the applied curvature, the mechanical bonding strength and the diameter to thickness ratios of the liner and outer pipe (Eq. (2)). In order to reduce liner wrinkling during spooling on, the mechanical bonding strength should be as high as possible. Further measures to reduce wrinkling are decreasing the applied curvature (increase the reel radius) and decreasing the diameter to thickness ratio of the liner pipe. Decreasing the diameter to thickness ratio of the outer pipe will result is lower ovalisation and thereby also have a beneficial effect on liner wrinkling.

$$a = f(\kappa), f\left(\sigma_{L;res}\right), f\left(d_{L;o}/t_L\right), f\left(d_{O;o}/t_O\right) \qquad (2)$$

In order to predict the residual liner wrinkling height as a result of spooling-on to all reel sizes larger than 5.5 m, of a 12.75 inch TFP (3 mm 316L liner and a 14.3 mm X65 outer pipe) without a TFP circumferential weld, with a residual liner hoop stress varying between 53 MPa (low) and 189 MPa (high), Eq. (3) can be used. In Eq. (3) only $f(\kappa)$ and $f(\sigma_{L;res})$ are addressed. $f(d_{L;o}/t_L)$ and $f(d_{O;o}/t_O)$ could not be addressed because only one value for $d_{L;o}/t_L$ and $d_{O;o}/t_O$ was tested. Eq. (3) is based on the best fit of the test results (Fig. 21).

$$a = \left((63.14\cdot\kappa)-\left(0.14\cdot e^{18.44\cdot\kappa}\right)\right)\cdot\left(\frac{189-\sigma_{L;res}}{189-53}\right)+\left(0.14\cdot e^{18.44\cdot\kappa}\right) \qquad (3)$$

MECHANICAL BONDING STRENTH AFTER REELING

The remaining average mechanical bonding strength in the TFP test pipes after spooling-on and unloading was measured using the API 5LD residual compressive stress test (Fig. 25) [14].

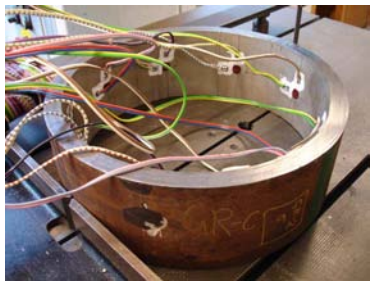

Figure 25 API 5LD residual compressive stress test

Test results indicated that the measured residual hoop and axial strains in the liner pipe were small and differed significantly in the circumference for all TFPs. The variation in measured strains could be attributed to changes in ovalisation between the situation where the strain gauges were attached to the liner pipe still inside the outer pipe and after saw cutting the outer pipe. Test results indicated as well that in the TFPs, either with a high or a low mechanical bonding strength a negligible average residual hoop and axial strains in the liner pipe remained after spooling-on and unloading. This means that in the TFP tested in this research, with either a high or a low mechanical bonding strength, a negligible average residual mechanical bonding strength remained after spooling-on and unloading.

The decrease of the mechanical bonding strength can be explained with the normality principle used in plastic theory [15]. After manufacturing TFP, a radial contact stress σ_C (i.e. the mechanical bonding strength) is present (point A in Fig. 26). Then, the TFP is bent during spooling-on and the bending moment (M) is increased until the yield surface is reached (point B). Further increases of the deformations have to obey the normality principle (the deformation vector at the yield surface). At point B this means decrease diameter $\Delta d_{L;a;TFP}$ and increase of the curvature κ. This means that the deformation vector at point B is not correct. The yield point gradually moves from point B via point C to point D in order the obey the normality principle. In point D the contact pressure σ_C is decreased to zero. In other words, the structure offers maximum resistance in the direction of deformation. In other directions where no deformation is applied, it does not need to maintain stresses.

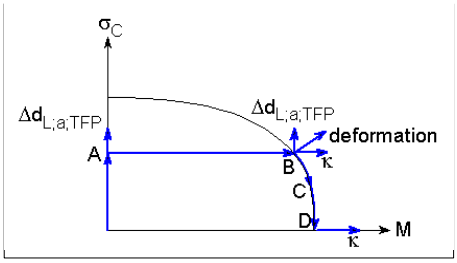

Figure 26 Yield surface for load case bending moment and contact pressure

These findings justify further research into this phenomenon as the eventual mechanical bonding strength after reeling installation may be vital for its anticipated application during operation.

CONCLUSIONS AND RECOMMENDATIONS

A 12.75 inch outer diameter single walled pipe bending test was executed and theoretical and FE analysis of this test was performed as preparation for 12.75 inch outer diameter TFP bending tests.

The main objective of the TFP bending tests was to determine the initiation and degree of liner wrinkling occurring during the TFP spooling-on phase when simulating the reeling pipelay installation method. Due to lack of a definition of liner wrinkling initiation, the crossing of a certain threshold of the liner wrinkle height was defined as liner wrinkling initiation. The bending tests results indicated that:

(1) the extent of liner wrinkling decreased if TFP with a high mechanical bonding strength was used.

(2) the presence of a circumferential weld in the highly bonded TFPs initiated higher liner wrinkles at lower curvatures than in case no circumferential weld was present.

(3) the ERW longitudinal outer pipe weld did not result in higher liner wrinkles.

API residual compressive stress tests showed that the initial mechanical bonding strength in the 12.75 inch TFP used in this research was significantly reduced, irrespective of whether a high or a low initial mechanical bonding strength had been used prior to spooling-on. These findings justify further research into this phenomenon as the eventual mechanical bonding strength after reeling installation may be vital for its anticipated application during operation.

Future research encompasses the FE analysis of these TFP spooling-on tests and the influence the spooling-on has on the significant reduction of the mechanical bonding strength between the liner and the outer pipe.

REFERENCES

[1] Koning, A. de, Nakasugi, H., and Li Ping, 2004, "TFP and TFT Back in Town (Tight Fit CRA Lined Pipe and Tubing)," Stainless Steel World, Jan/Feb, pp. 53-61.

[2] Mizumura, M., Hiroyuki, H., Naoi, H., and Higashiyama, H., 1992, "Behaviour of Mechanically Bonding Double Wall Pipe under Various Loading Conditions," Proceedings of the 2nd International Offshore and Polar Engineering Conference, pp. 142-150

[3] Focke, E.S., Gresnigt, A.M., Meek, J., and Nakasugi, H., 2005, Experimental Behaviour on Local Buckling Behaviour of Tight Fit Pipe, Proceedings of the 15th International Symposium of Offshore and Polar Engineering, pp.76-84

[4] Focke, E.S., Gresnigt, A.M., and Meek, J., 2006, Small Scale Reeling Tests, Proceedings of the 16th ISOPE Conference, pp.118-126

[5] API, 2004, Specification Line Pipe API Specification 5L American Petroleum Institute, 43rd Edition

[6] NEN, 2003, Staal Katern 6 Bijlagen E en F, NEN 3650-2

[7] Gresnigt, A.M., 1986, Plastic Design of Buried Pipelines in Settlement Areas, HERON, Volume 31, No.4

[8] ABAQUS Analysis User's Manual, ABAQUS, Inc.

[9] Karjadi, E, 2006, Full Scale Bending Tests for Reeling Simulation of Single Walled Pipe: Experiment vs ABAQUS Calculation, ABAQUS Benelux User's Meeting 2006, Leuven, Belgium, November 16-17, 2006

[10] DNV, 2000, Offshore Standard OS-F101 Submarine Pipeline Systems, Det Norske Veritas

[11] Murphey, C.E. and Langner, C.G., 1985, Ultimate Pipe Strength under Bending, Collapse and Fatigue, Proceedings of the 4th International Conference on Offshore Mechanics and Arctic Engineering, pp.467-477

[12] Levold, E., Vitali, L. and Mørk, K., 2005, Submarine Pipeline Installation JIP: Strength and Deformation Capacity of Pipes Passing over the S-lay Stinger, Proceedings of the 25th International Conference on Offshore Mechanics and Arctic Engineering, pp.1-9

[13] DNV, 2005, Reel Installation of Clad Steel Pipe, DNV Pipeline Committee 18.02.2005, Det Norske Veritas

[14] API, 1998, Specification for CRA Clad or Lined Steel Pipe, API Specification 5LD American Petroleum Institute, 2nd Edition

[15] Gresnigt, A.M., 1986, Plastic Design of Buried Pipelines in Settlement Areas HERON, Volume 31, No.4